ACS APPLIED MATERIALS & INTERFACES

Research Article

www.acsami.org

Chelating Surfaces for Native State Proteins Patterning: The Human Serum Albumin Case

Nicoletta Giamblanco, Nunzio Tuccitto,* Gabriella Zappalà, Gianfranco Sfuncia, Antonino Licciardello, and Giovanni Marletta

Laboratory for Molecular Surfaces and Nanoscience (LAMSUN), Department of Chemical Sciences, University of Catania and CSGI, Viale Andrea Doria 6, 95125, Catania, Italy

ABSTRACT: The paper reports a new "soft" surface functionalization strategy, based on a highly selective ion metal chelation process. The proposed stepwise methodology implies at first the construction of a monolayer of terpyridine-based thiol (Tpy), whose highly packed structuring has been followed in situ by using quartz crystal microbalance (QCM-D) measurements, showing that the monolayers consist of about 2.7×10^{14} Tpy/cm^2. Then, the tridentate sites of the each Tpy moiety are employed to partially chelate divalent metal ions, providing an effective platform to anchoring proteins by completing the metal ion coordination with an available site on the protein of interest. We report the case study of the application of the process to the HSA immobilization onto various surfaces, including Tpy−Fe(II) and Tpy−Cu(II) complexes, as well as hydrophilic bare gold substrates and hydrophobic self-assembled Tpy-based monolayers. It is shown that the chelation interaction between Tpy−Cu(II) complexes and HSA produces the highest and most robust HSA immobilization, with an adsorbed mass at the steady state of ∼800 ng/cm^2, with respect to an average adsorption of ∼350 ng/cm^2 for the other surfaces. Furthermore, Cu(II)-chelated surfaces seem to promote a sort of protein "soft" landing, preventing the ubiquitous surface-induced major unfolding and transmitting an orientation information to the protein, owing to the highly specific symmetry coordination of the Tpy−Cu(II)−protein complex. Indeed, the interaction with a specific monoclonal antiboby (anti-HSA) indicated the lack of a significant protein denaturation, while a massive reorientation/denaturation process was found for all the remaining surfaces, including the Tpy−Fe(II) complex. Finally, the metal-ion-dependent HSA immobilization selectivity has been exploited to obtain micropatterned surfaces, based on the strikingly different strength of interaction and stability observed for Fe(II) and Cu(II) complexes.

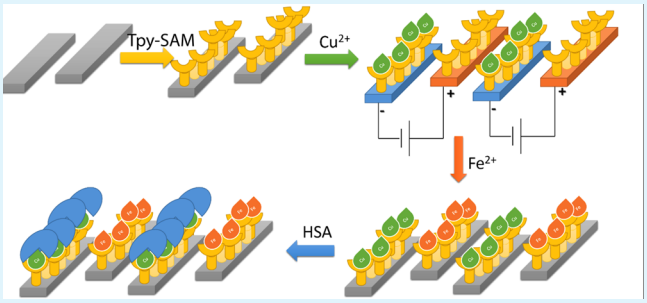

KEYWORDS: *chelation, metal complexes, surfaces, human serum albumin, patterning, interdigitated electrodes, terpyridine*

1. INTRODUCTION

Protein interactions with solid synthetic or natural surfaces have implications in fields as pervasive as biomaterials, biosensing, drug delivery, and immunoassays.[1] Indeed, a continued research activity has been undertaken to develop new biomaterials for use in reconstructive implants,[2−5] new tissue engineering strategies,[6,7] advanced biosensing,[8,9] and drug delivery devices.[10] All these applications require a thorough understanding of favorable or adverse biological reactions, which are mediated by adsorbed proteins, in view of optimizing the response of the biological systems.[11,12] Moreover, a general prerequisite for successful applications implies stable protein structures at the surfaces and in turn the control of folding and unfolding processes. In fact, proteins often are denatured at solid−liquid and air−liquid interfaces, although they retain more structure on neutral hydrophilic surfaces than on charged or hydrophobic surfaces.[13] Denaturation, in fact, affects the proper biofunctionality of the immobilized biomolecules, critically dependent upon the spatial accessibility of the relevant protein epitopes.[14,15] In this context, it gradually became clear that it is mandatory to achieve the control of the state of the adsorbed proteins and in turn to develop reliable methods to achieve the desired native conformation and/or orientation of proteins at synthetic or natural surfaces and interfaces.[16−20]

The immobilization of proteins is generally obtained by two main strategies, respectively consisting of simple "soft" physisorption-based processes, which basically exploit aspecific interactions yielding the random orientation of the immobilized proteins, or of "hard" chemisorption strategies, basically implying specific and directional bonding, inducing the adoption of specific and "constrained" conformation reorganization modes. In this scenario, the development of a "soft" chemisorption strategy for native state and oriented protein anchoring would be a breakthrough in producing "naturally" biofunctional surfaces.

A promising methodology to fulfill the requirement of "softly" linking proteins to a given substrate is the ion metal−protein chelation. Indeed, in previous papers we have

Received: September 2, 2015
Accepted: October 1, 2015
Published: October 1, 2015

DOI: 10.1021/acsami.5b08217
ACS Appl. Mater. Interfaces 2015, 7, 23353−23363

Scheme 1. Schematic Representation of the Patterning Procedure

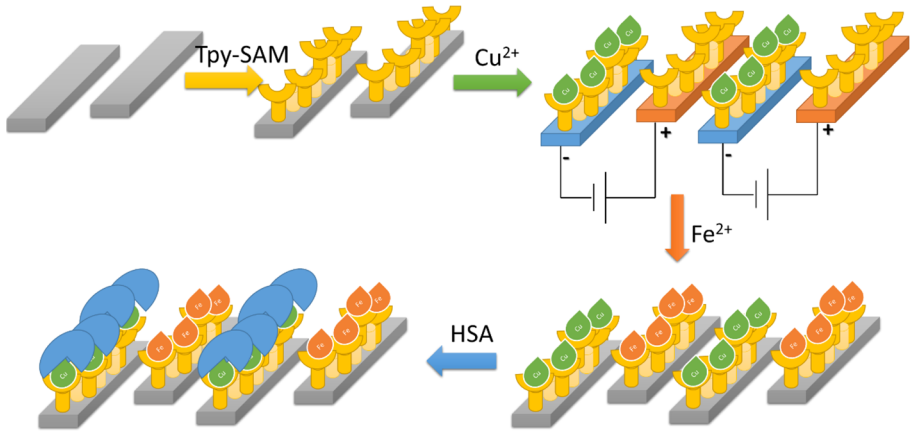

demonstrated that surface anchoring and patterning of proteins were achieved by using an original strategy exploiting the spontaneous chelation-induced interaction between biomolecules and iron complexes.[21−23] In agreement with the "softness" of the linking, such an approach does not involve any chemical modification of the pristine biomolecule. The efficiency of the strategy to functionalize nanoporous polymeric membranes was further demonstrated.[24]

In the present paper we report the "soft" selective ion metal chelation-based immobilization and patterning of human serum albumin (HSA) onto gold surfaces. The present paper deals mainly with a novel, crucial, and biologically relevant finding concerning the surprising efficiency in preventing the usual, spontaneous denaturation processes. The process we report not only yields a strong ion-related selectivity in protein anchoring but also determines the "soft" immobilization in protein native state.

HSA has been used for the present proof-of-concept work in view of its wide biotechnological applications, including implantable biomaterials, surgical adhesives and sealants, ligand trapping, and fusion proteins. Indeed, HSA displays an extraordinary ligand binding capacity, representing the main carrier for fatty acids, affecting pharmacokinetics of many drugs, providing the metabolic modification of some ligands, and rendering potential toxins harmless.[25] Furthermore, HSA is a valuable biomarker of many diseases, including cancer and rheumatoid arthritis,[26] and it is widely used clinically to treat a large number of diseases.[25] In view of these many aspects, the setup of a general-purpose platform capable of trapping fully bioactive HSA appears as a highly valuable achievement.

HSA can bind a multitude of metal ions, among which is particularly relevant the interaction with Cu^{2+}.[27−32] Accordingly, we have employed a monolayer of copper(II)-chelated terpyridine thiols to link native HSA. Indeed, by using the selective recognition of native state HSA by means of monoclonal antibody (anti-HSA), we could demonstrate that the natural Cu(II) metal−protein interaction allows a sort of "soft" protein landing on the Cu(II)-chelated surface, preventing the typical protein denaturation occurring at unspecific surfaces, like the hydrophobic terpyridine self-assembled monolayer, the hydrophilic UV−O_3 treated gold substrates, as well as the iron-chelated self-assembled terpyridine monolayers. Finally, a robust and stable micropattern of native state HSA could be demonstrated by patterning different chelating ions (Cu(II) vs Fe(II)) onto interdigitated electrodes.

2. EXPERIMENTAL SECTION

2.1. Materials. [4′-(4-Mercaptophenyl)-2,2′:6′2″-terpyridine], a thiol-functionalized terpyridine-based ligand (Tpy), was synthesized on purpose,[37] whereas mercaptobenzene (MB) was commercially available (Aldrich, Milan, Italy). We purchased human serum albumin (HSA), copper(II) sulfate, iron(II) sulfate, ethanol (for HPLC, gradient grade, ≥99.8%) from Aldrich (Milan, Italy) and used as delivered. We prepared water-based solutions by using filtered ultrapure water (Millipore Milli-Q, Merck S.p.a, Milan, Italy). We used 100 nm thick gold films as substrates to prepare unpatterned SAM (Aldrich, Italy). We purchased interdigitated gold-based microelectrodes fabricated by thin-film technologies on a glass substrate from Micrux-Technologies (Oviedo, Asturias, Spain). An amount of 9.0 μg of monoclonal anti-human serum albumin (monoclonal anti-human serum albumin clone HSA-11, A 6684, Aldrich, Italy) was dissolved in 1 mL of pure water.

2.2. Preparation of Protein Films. We prepared mixed component SAMs by immersion of the substrate (cleaned in UV−ozone atmosphere for 600 s and then rinsed in ethanol) in an ethanol solution of thiol-functionalized terpyridine-based ligand (Tpy) and mercaptobenzene in equimolar concentration ratio for 24 h. We washed samples with ethanol, and then we dried them with a nitrogen stream. Cu(II) and Fe(II) terpyridine-based complexes were prepared by immerging Tpy-based self-assembled monolayer in $CuSO_4$ and $FeSO_4$ solution for 15 min (10^{-3} M, ethanol/water 1:1). We washed samples with ethanol, and then we dried them with a nitrogen stream. We dipped SAMs in HSA solution with a concentration of 10.0 μg/mL (i.e., 0.14 μM) for 15 min. Finally, we rinsed samples with water and then we dried them with a nitrogen stream.

2.3. Complex Patterning. The strategy to prepare surface patterning of Cu(II) and Fe(II) complexes is sketched in Scheme 1. First, we assembled terpyridine-based SAMs onto arrays of interdigitated gold electrodes (IDEs). Subsequently, we applied 1.0 V (dc) between the two series of golf fingers and then we dipped them in Cu^{2+} containing solution to form Cu(II)-complex SAMs selectively at the negative biased electrodes. The immersion time in Cu(II) containing solutions was always less than 5 s. Different bias voltages and immersion times are still under investigation. After that, we immersed IDEs in a Fe(II) containing solution without any dc bias. We dipped SAMs in HSA solution with a concentration of 10.0 μg/mL (i.e., 0.14 μM) for 15 min. Finally, we rinsed samples with water, and then we dried them with a nitrogen stream.

2.4. Samples Characterization. QCM-D measurements were performed by means of the Q-Sense E1 systems: Au coated quartz sensor, AT-cut 5 MHz gold quartz crystals, diameter 14 nm, and thickness 0.3 mm from Q- Sense AB (Goteborg, Sweden). Before use, all the gold crystals were cleaned by UV−O_3 treatment for 20 min and

DOI: 10.1021/acsami.5b08217
ACS Appl. Mater. Interfaces 2015, 7, 23353−23363

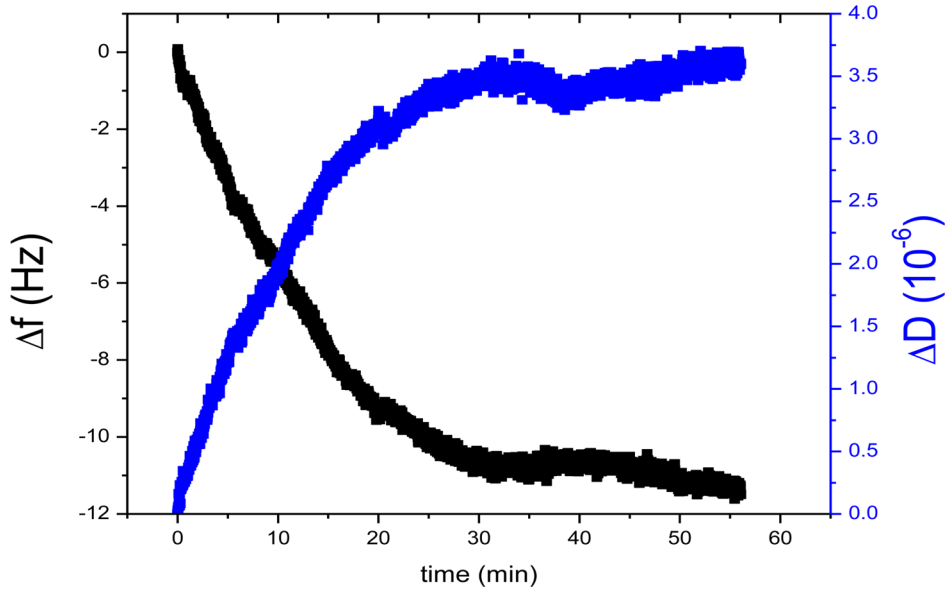

Figure 1. Frequency (Δf) and dissipation (ΔD) shift as a function of the adsorption time of mixed MB−Tpy SAM onto QCM-D gold sensor.

then rinsed with water and ethanol and finally dried with a stream of nitrogen gas. All the measurements were carried out in triplicate at 25 °C. We studied the in situ adsorption of mixed Tpy-based monolayers on gold surface of the QCM-D sensor. To study the protein adsorption on Cu(II) and Fe(II) complexes, we prepared complexes-based SAMs ex situ onto QCM-D sensors. Then the HSA adsorption was recorded in situ allowing the protein to interact with the sensor modified surfaces. The Sauerbrey relation was used to calculate mass adsorbed.[33,34]

Surface plasmon resonance measurements were performed with an SPR Navi 200-L instrument equipped with one light at 670 nm wavelength (BioNavis Ltd., Tampere, Finland). SPR sensors were gold-coated sensors (50 nm) with a chromium adhesion layer (~2 nm) and were obtained from BioNavis Ltd. SPR sensors were cleaned before use by boiling them for 15 min in an NH_4OH (30%)/H_2O_2 (30%)/H_2O (1:1:5, v/v) oxidizing solution. Data modeling for sample layer analysis was done by using the Winspall software. The thickness of Tpy-based SAM was extracted by fitting the intensity versus angle curves assuming a refractive index of n = 1.445.[35,36]

ToF-SIMS analysis was performed with a TOFSIMS-IV (ION TOF Gmbh, Muenster, Germany) time-of-flight secondary ion mass spectrometer. Spectra were obtained by using a pulsed 25 keV Bi^+ primary ion beam from a liquid metal ion source. Primary ion fluence was kept lower than 5×10^{12} ions per cm^2 in order to ensure static SIMS conditions. Mass resolution ($m/\Delta m$) was typically >8000 at m/z = 28 in both positive and negative ion modes. Mass resolved images (chemical maps) were typically acquired by rastering the primary beam over an area of 100 μm × 100 μm with a digital resolution of 256 × 256 pixels.

Atomic force microscopy (AFM) images were acquired in contact mode. Nanoprobe cantilevers (100 and 200 mm standard spring constants ranging from 0.12 to 0.52 N/m) with oxide-sharpened Si_3N_4 integral tips (Veeco NanoProbe Tips NP-20) were used. The applied force was varied over a wide range from several nanonewtons up to tens of nanonewtons. Stripe thickness was estimated by means of histogram (bearing) analysis.

The surface wettability was traced by measuring the static water contact angle (WCA). An OCA30 instrument (Dataphysics) was used at 25 °C and 65% relative humidity. Probe liquid drops of 2 μL of volume were applied on different zones of each sample surface, and by digital image analysis, the static contact angles were measured on both sides of the 2D projection of the droplet. At least three measurements were made for each sample and then averaged.

3. RESULTS AND DISCUSSION

3.1. Chelating Platforms. The platforms to achieve chelation-induced interaction between proteins and metal complexes were optimized by using a preliminary SAM-based strategy to functionalize microcrystalline gold surfaces. In particular, an effective and uniform surface functionalization was achieved by preparing a stable and reproducible mixed self-assembled monolayer of terpyridine-based chelating ligand (Tpy) and mercaptobenzene (MB) molecules as lateral spacers. This system actually acts as a versatile "platform" for surface anchoring of metal complexes by direct coordination reaction at the terpyridine sites. We have previously reported on the unusual behavior of this mixed component system on gold, which has the tendency to assume a surface composition that is almost independent, in a wide composition range, on the ratio of the two constituents (MB and Tpy) in the solution used for the self-assembling process.[37−44] Accordingly, the experimental ratio of the two components at the surface, measured by XPS and TOF-SIMS, is approximately 1:1. This is interpreted in terms of the formation of a stable structure owing to the strong lateral MB−Tpy interaction.[38]

In the present paper, in order to measure the number of surface-bonded chelating molecules, we followed the formation of the mixed MB−Tpy monolayer at the gold surface by quartz crystal microbalance with dissipation monitoring (QCM-D). Figure 1 shows the frequency shift during the first step of the thiols adsorption on the surface.

The frequency shift (Δf) has been evaluated by means of the Sauerbrey equation, providing an estimate of the adsorbed mass at the steady state of about 203.0 ± 5.0 ng/cm^2. The non-negligible dissipation value at the steady state is diagnostic of the occurrence of a dynamic reorganization process of the adsorbing thiol molecules at the gold surfaces. As the component ratio of the bonded monolayer is known to be 1:1,[37] we can consider the monolayer formed by "super-molecules", consisting of a virtual dimer MB−Tpy, with a global pseudomolecular weight of 451 g/mol. In this frame-work, each "supermolecule" corresponds to a chelating unit and the total number of them is 2.7×10^{14} units/cm^2. The calculated area per MB−Tpy dimer is 0.37 (±0.04) nm^2, which

DOI: 10.1021/acsami.5b08217
ACS Appl. Mater. Interfaces 2015, 7, 23353−23363

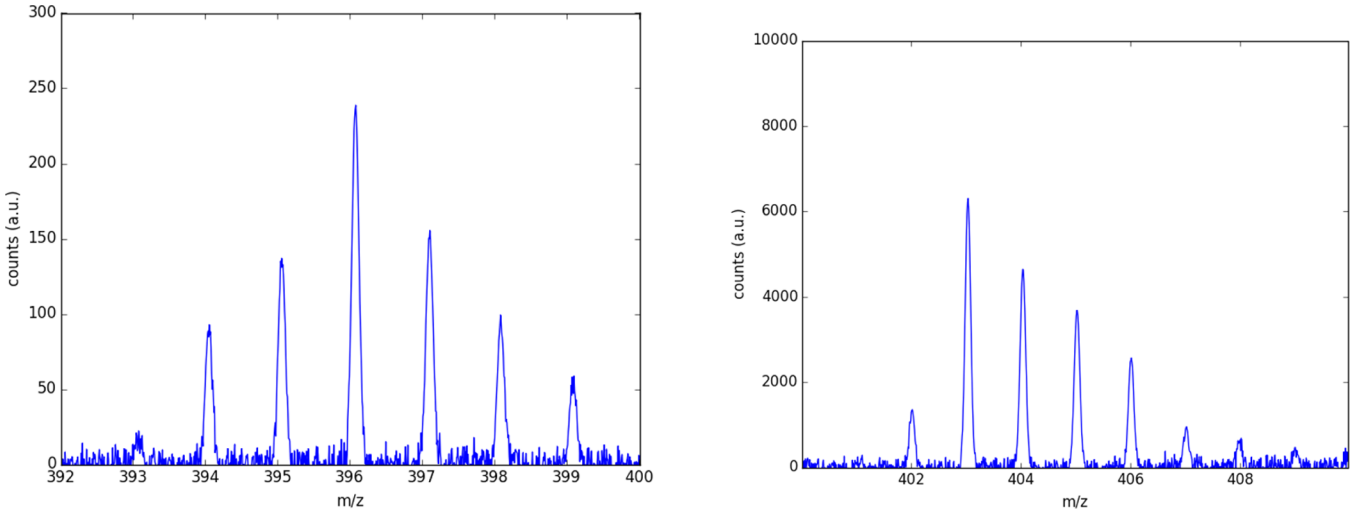

Figure 2. Portion of positive ToF-SIMS spectra of Fe(II)- and Cu(II)-based SAMs (left and right, respectively).

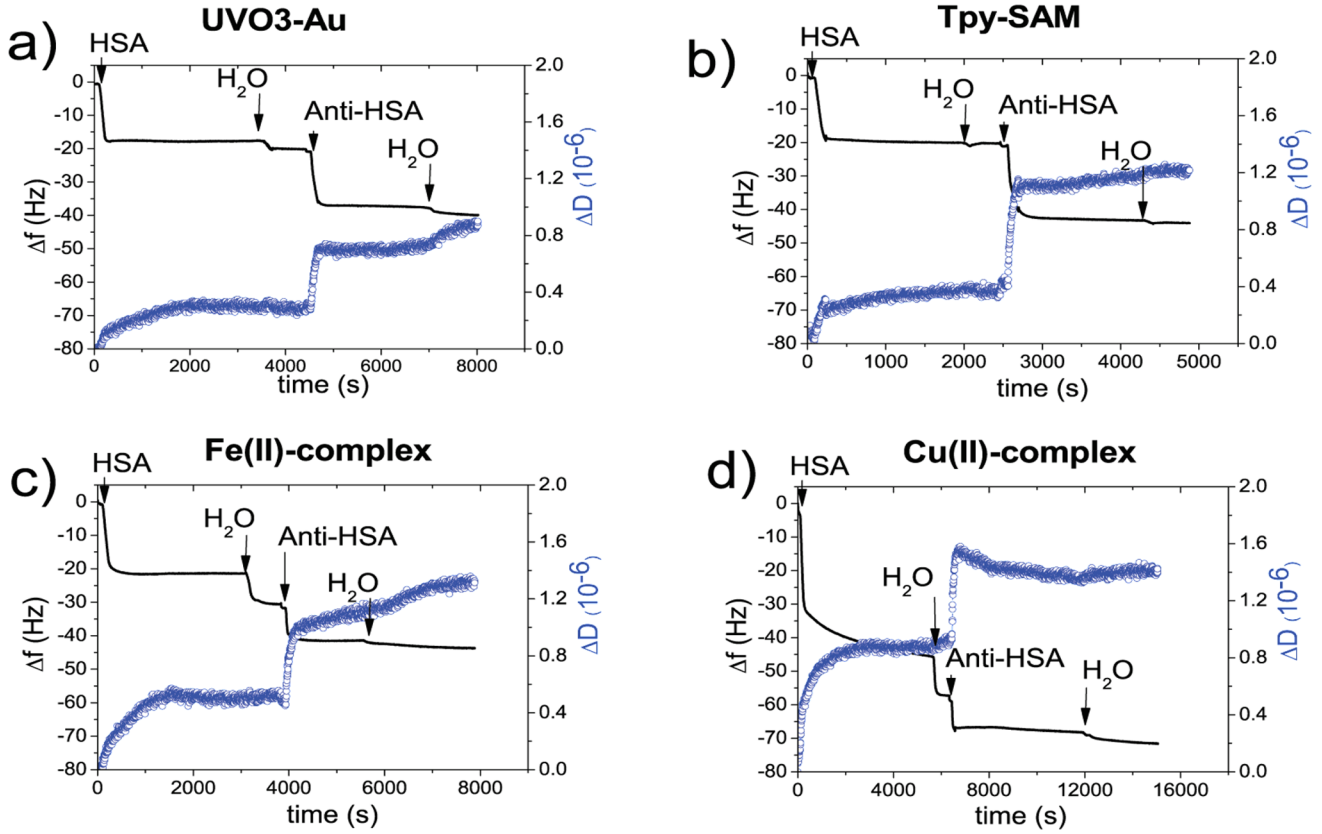

Figure 3. Frequency (Δf) and dissipation (ΔD) shift as a function of the adsorption time of HSA followed by anti-HSA onto (a) UVO_3-gold, (b) Tpy−SAM, (c) Fe(II)-complex, (d) Cu(II)-complex. The arrows indicate anti-HSA and water rinsing times.

is fairly close to the theoretical value of 0.43 nm^2 expected per an "intercalated" herringbone $(\sqrt{3} \times \sqrt{3})R30°$ organization of MB−Tpy.[45]

Further confirmation of the equimolecular nature of the formed monolayer was obtained by measuring the thickness of Tpy-based SAM by means of surface plasmon resonance (SPR). In fact, the measured value is 1.3 ± 0.1 nm, in close agreement with the expected height of Tpy molecules in the above-mentioned herringbone $(\sqrt{3} \times \sqrt{3})R30°$ orientation. It is worth mentioning that the very same result has been obtained by angular dependent NEXAFS analysis.[39]

Finally, the chelating platform has been finalized by performing a step of formation of selected metal complexes. In particular, Cu(II) and Fe(II) have been used in view of the different behavior of the protein moiety with respect to them. The terpyridine-based metal complexes were prepared by simple dipping step (see Experimental Section).

The stepwise formation of Fe(II) and Cu(II) complexes was confirmed by ToF-SIMS analysis, showing the presence of large mass peaks assigned to quasi-molecular fragments of respectively Tpy−Fe $(C_{21}H_{14}N_3SFe)^+$ (at m/z = 396) and

DOI: 10.1021/acsami.5b08217
ACS Appl. Mater. Interfaces 2015, 7, 23353−23363

Tpy−Cu $(C_{21}H_{14}N_3SCu)^+$ (at m/z = 403) in the spectra of positive ions, as shown in Figure 2.

3.2. Protein Chelation. The interaction of HSA with bare hydrophilic gold surface, i.e, treated by UVO_3 (henceforth indicated as UVO_3-Au), terpyridine-terminated self-assembled monolayer (Tpy−SAM), surface-anchored Fe(II) and Cu(II) terpyridine-based complexes was monitored in situ and in real time by using QCM-D. In order to assess the retention or loss of the biological activity of the anchored HSA on the various surfaces, also their response to an HSA-monoclonal antibody (anti-HSA) has been sequentially determined for each surface in the same experiment. Indeed, the employed monoclonal antibody reacts specifically against denatured human albumin.

UVO_3-Au is a hydrophilic surface having water contact angle (WCA) of around 10°. Tpy−SAM is relatively hydrophobic with WCA ≈ 80°. Both surfaces are used as blank substrate, in view of the nonspecific character of their interaction with HSA, whereas Fe(II)-complex and Cu(II)-complex SAM, which both exhibit similar WCA values, i.e., ∼50°, are employed to study their specific chelation behavior of HSA.

As illustrated in Figure 3, HSA has a quantitatively similar interaction with hydrophilic UVO_3-Au and hydrophobic Tpy−SAM, yielding an adsorbed mass of about 310.0 ± 6.0 ng/cm^2 for UVO_3-Au and about 330.0 ± 7.0 ng/cm^2, with a negligible dissipation ($D \cong 0.2 \times 10^{-6}$).

By contrast, HSA has a much stronger interaction with the Cu(II)-complex SAM than for Fe(II)-based ones and the blank reference surfaces (UVO_3-Au and Tpy). Indeed, the frequency shift at the steady state onto Cu(II)-complex is about 800.0 ± 16.0 ng/cm^2, i.e., more than twice the steady value for Fe(II)-complex of about 370.0 ± 7.0 ng/cm^2, and 310.0 ± 6.0 ng/cm^2 for UVO_3-Au and about 330.0 ± 7.0 ng/cm^2 for Tpy. Finally, also the dissipation is comparatively higher, indeed $D \cong 0.4 \times 10^{-6}$ for HSA adsorbed onto Fe(II)-complex and $D \cong 0.8 \times 10^{-6}$ for the almost double HSA adsorbed mass on Cu(II)-complex. In other words, it appears roughly parallel to the differential adsorbed mass. Moreover, by taking into account the fact that the adsorption is very similar for the hydrophilic (UVO_3-Au) and hydrophobic surfaces (TPY−SAM) and rememberingg that the WCA for the Fe (II) and Cu(II)-complex surfaces are very similar (i.e., mildly hydrophilic behavior), the relevance of a supposable pure hydrophobic effect in the case of the HSA adsorption onto Cu(II)-complex surfaces is ruled out.

The strength of interaction of HSA with respectively Cu(II) and Fe(II) chelating ions may be understood on the basis of the discussion of the type of binding sites in physiological conditions and in solution. Paramagnetic Cu(II) ions are known to form strong tetragonal complexes with biological nitrogen ligands.[46] In particular, HSA contains four metal binding sites, vastly differing in structure and metal ion specificity. They are the N-terminal site (NTS, also known as ATCUN), Cys34 residue, and its environment, site A identified in NMR studies (and later shown to be identical with the multimetal binding site (MBS)), located at the interface of domains I and II, and site B.[33] The most important Cu(II)-binding site is the N-terminal site (NTS), composed of the first three residues of albumin sequence, e.g., Asp-Ala-His in human protein.[47] The main feature of this binding site for chelation in solution is the involvement of peptide bond nitrogens in the metal ion coordination, enabled by a simultaneous presence of the free N-terminal amine and His-3. This four-coordinate arrangement of donor atoms prefers metal ions capable of square planar complex formation, e.g., Cu(II) and Ni(II).[46,48] In the case of surface-anchored Cu(II) ions, we suggest that the terpyridine is providing three of the complexing nitrogens, while HSA provides the free N-terminal amine from the NTS site, as drawn in Scheme 2. Indeed, the N-terminal amino group

Scheme 2. Tentative Schematic Representation of HSA NTS-Cu(II) Complex in Solution[44] (Left) and Cu(II)−Tpy−HSA Complex at Interface (Right)

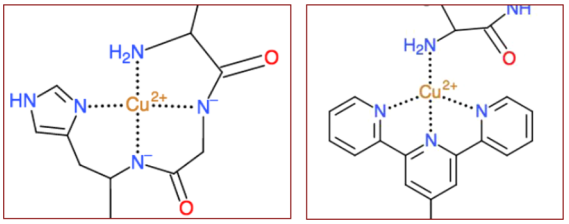

of NTS motif is characterized by a very good affinity for soft and intermediate metal ions, like Cu^{2+}, Zn^{2+}, or Ni^{2+}. In view of the very high stability of the Cu(II)−HSA complexes, we propose that further specific Cu(II) binding site in albumins (i.e., site A) is not significantly involved in the complexation process. In fact, the 10 000-fold difference of Cu(II) affinities between NTS and MBS/site A suggests that only NTS is populated by Cu(II) under physiological conditions. On the other hand, it has been reported that Fe(II) binds to HSA only if it is maintained in the reduced Fe(II) form, e.g., in the presence of ascorbate, but the binding is nonspecific and occurs at the protein surface. Accordingly, these arguments apparently indicate that if some site B interaction cannot be excluded, the binding at NTS, MBS/site A, or Cys34 does not occur. All of this supports our proposal that HSA binds Cu(II) essentially with the free N-terminal amine at the NTS site.[44]

The analysis of the HSA adsorption kinetic onto the various surfaces shows significant differences in the protein−surface interaction process. In particular, for UVO_3-Au, Tpy, and Fe(II)-based SAMs, the initial adsorption is fast and a steady-state plateau is quickly reached. By contrast, the adsorption of HSA onto Cu(II)-based SAMs occurs in two well distinct steps, the first one consisting of a rapid adsorption, as in fact expected for the high affinity expected for Cu(II) and HSA, the second one being much slower.

Figure 4 reports the fitting curves and parameters of the QCM-D isotherms. As shown in the figure, the HSA adsorption on UVO_3-Au, Tpy−SAM, and Fe(II)-complex data are well fitted by the pseudo-first-order eq 1:

$$\Delta F_t = \Delta F_1(1 - e^{-k_1 t}) \quad (1)$$

where ΔF_t and ΔF_1 are the frequency shifts associated with the protein adsorption at any time t and at equilibrium, respectively, and k_1 is the kinetic rate constant.

At variance of the above behavior, the data from HSA adsorption onto Cu(II) are well fitted by a biexponential equation:

$$\Delta F_t = \Delta F_1(1 - e^{-k_1 t}) + \Delta F_2(1 - e^{-k_2 t}) \quad (2)$$

where ΔF_1 and ΔF_2 are the frequency shifts associated with the two steps of the protein adsorption process, and k_1 and k_2 are the kinetic rate constants.

The rate constant k_1 in eq 1 is commonly interpreted as describing the ratio of adsorption and desorption rate

DOI: 10.1021/acsami.5b08217
ACS Appl. Mater. Interfaces 2015, 7, 23353−23363

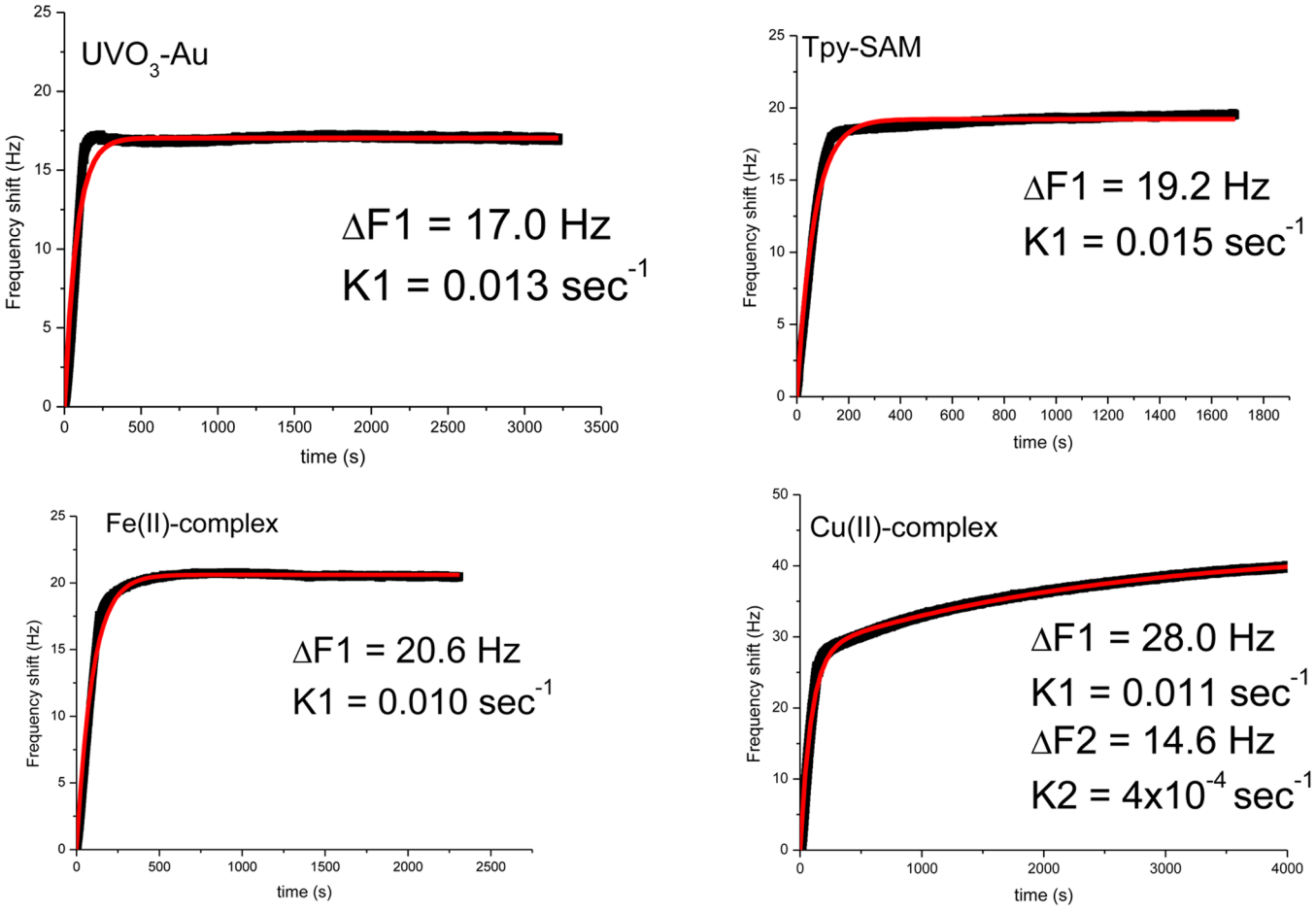

Figure 4. Inverse frequency−time diagrams for UVO_3-Au, Tpy−SAM, Fe(II)-complex, Cu(II)-complex. Fitting parameters (ΔF_1, k_1, and ΔF_2, k_2) are reported in the insets in the figure.

constants.[49] In the biexponential case, instead, there is no common agreement on the meaning of the two rate constants k_1 and k_2, also if it has been proposed that the fast reaction rate k_1 corresponds to the effective binding interaction of the molecule of interest, strictly related to the kinetics facts. On the other hand, the slower reaction rate k_2 has been suggested to depend on steric hindrance effects, shape rearrangements, or surface diffusion limitations.[50,51] It is noteworthy that the k_1 values related to HSA binding on UVO_3-Au, Tpy−SAM, and Fe(II)-complex are virtually similar to the k_1 value obtained by fitting the initial fast adsorption process of HSA binding on Cu(II) terpyridine-complex, indicating that the primary adsorption process is driven by similar interaction forces and similar accessibility to the chelating sites. This initial fast step of HSA absorption onto Cu(II)-complex implies that about 3/4 of the total mass uptake is achieved, while the remaining quarter is adsorbed during the subsequent almost 2 orders of magnitude slower step ($k_2 \ll k_1$). The two different kinetic processes for HSA seem to correlate nicely with the relative availability of the two different chelation sites of HSA toward Cu(II), yielding two different chelation constants.[52,53] In our experiment, dealing with Cu(II) chelating sites immobilized on surfaces, the fast step has a k_1 value of 0.01 s^{-1} and k_2 has a value of 1×10^{-4} s^{-1}.

Further hints on the chelation kinetics can be obtained from the analysis of the change in the dissipation values (ΔD) for the adsorbed HSA layers on the various surfaces. Generally, soft films show high dissipation values and rigid films exhibit small dissipation values. Commonly, as ΔD values lower than 1×10^{-6} are considered diagnostic of rigid films,[54] the measured dissipation values for HSA-adsorption suggest that rigid layers are indeed formed on the various surfaces. However, the detailed analysis of the relationship between ΔF and ΔD showed that a significant difference occurs for the adsorption of HSA onto Cu(II)-complexes surfaces. This analysis can be performed by plotting ΔD vs ΔF ($D-F$ plots), as reported in Figure 5. The $D-F$ plots remove time as an explicit parameter and put in evidence, via the slope of the curves, the relative dissipation change for a given frequency shift, i.e., the energy dissipation response for a given amount of adsorbed mass to the shear stress imposed by the sensor oscillation.

According to the theory, in the limits of the Sauerbrey conditions validity, a linear dependence is expected for rigid layers, as it is indeed observed for the first part of the $D-F$ plots of UVO_3-Au, Tpy, and Fe(II)-complex surfaces in Figure 5. It noteworthy that the slopes of the three straight lines obtained for these three surfaces, notwithstanding their marked differences (different wettability, surface charging, chemical composition, etc.), are roughly the same, confirming that a very similar adsorption process occurs in the three cases. After this first build-up step, reaching the mass steady state, the lines go parallel to the y-axis (ΔD), indicating that the stationary adsorbed mass undergoes a continuous increase of dissipation.

DOI: 10.1021/acsami.5b08217
ACS Appl. Mater. Interfaces 2015, 7, 23353−23363

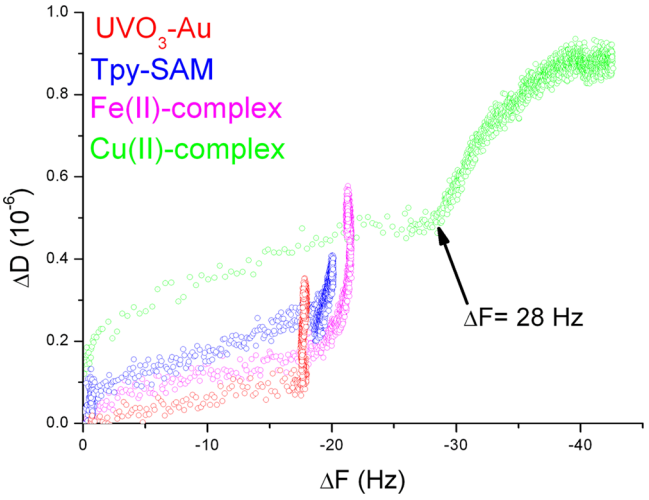

Figure 5. ΔD vs ΔF plots for HSA adsorption onto UVO_3-Au (red), Tpy−SAM (blue), Fe(II)-complex (purple), and Cu(II)-complex (green).

This is interpreted, in agreement with literature,[55] in terms of the drastic reorientation/degradation of the adsorbed proteins.

By contrast, when HSA is allowed to adsorb onto Cu(II)-complex, the related $D-F$ plot is completely different. Figure 5 shows that during the first quasi-linear step, while the $D-F$ slope is very similar to the ones of the UVO_3-Au, Tpy, and Fe(II)-complex surfaces, the HSA layer onto Cu(II)-complex is markedly more dissipative (about twice) than the layers on the three surfaces mentioned above. Furthermore, a second adsorption step occurs, as indicated by a second curve in the $D-F$ plot, reaching a stable dissipation steady state, diagnostic of the absence of a significant protein reorientation/denaturation. Noticeably, the discontinuity point of the Cu(II)-complex related curve occurs at a frequency shift of about 28 Hz, i.e., at the very same value calculated from the above-described time-dependent kinetic fitting.

Overall, the data reported until now indicate that while the adsorption process onto UVO_3-Au, Tpy, and Fe(II)-complex surfaces (henceforth indicated as "unspecific surfaces") reaches a steady state at roughly the same low adsorbed mass for the three surfaces, a much higher mass is adsorbed onto Cu(II)-complex surfaces (henceforth indicated as "specific surfaces"). Furthermore, the kinetic and $D-F$ analysis suggest that HSA adsorbs roughly in the same way, i.e., in a single fast step with very similar kinetic constants for all the unspecific surfaces, undergoing a massive reorientation/denaturation process, as figured out from the drastic dissipation increase at the steady adsorbed mass. On the contrary, HSA adsorbs onto the specific surfaces by means of a very peculiar kinetics, based on the process of binding through the Cu(II)-chelation sites, occurring in two subsequent steps, respectively involving a first fast process, where HSA molecules are soft landing on the surface without reorganization, and a second much slower process, where further HSA molecules land, saturating the adsorption at higher HSA coverage.

These three findings together point toward the occurrence for the unspecific surfaces of a common adsorption-and-denaturation process, driven by the widely reported drastic conformational rearrangement/spreading of the adsorbed HSA molecules.[56] This process is characterized by a complete surface saturation with the rearranged molecules, which in turn blocks any further HSA uptake.

On the other hand, the HSA soft immobilization for the specific surfaces, according to the above-discussed data, apparently does not involve any significant HSA reorganization, allowing a better packing of the adsorbed molecules and prompting a higher number of bound molecules.

The above picture agrees with the evaluated HSA surface coverage for the various surfaces. In fact, for the case of unspecific surfaces we have found the following number of molecules/cm^2: 2.8×10^{12} molecules/cm^2, 3.0×10^{12} molecules/cm^2, and 3.3×10^{12} molecules/cm^2, respectively, for UVO_3-Au, Tpy−SAM, and Fe(II)-complex, while for the specific surfaces the adsorbed HSA corresponds to 7.2×10^{12} molecules/cm^2. Assuming a protein film density[57] of 1300 kg/m^3,[58] which takes into account a contribution of 25% of trapped water,[56] we estimated an "effective" adsorbed layer thickness: 2.4 ± 0.1 nm, 2.5 ± 0.1 nm, and 2.8 ± 0.1 nm, respectively for UVO_3-Au, Tpy−SAM, and Fe(II)-complex surfaces, while for the specific ones it is about 6.2 ± 0.2 nm. These "effective" thickness data, when compared with the native state albumin dimensions of $4 \times 4 \times 14$ nm^3,[59,60] suggest that for unspecific surfaces the adsorbed HSA molecules are basically spread/unfolded, while for the specific surfaces it is suggested that a native conformation, possibly involving a side-on adsorption mode, is obtained.

The denatured vs native state of the HSA immobilized on the two different types of surfaces can be confirmed by means of a very selective recognition process based on the use of a monoclonal HSA-antibody (anti-HSA), specifically sensitive to the conformational state of the adsorbed proteins. Indeed, the selected antibody reacts specifically only against denatured human serum albumin.[61] The anti-HSA uptake has been followed by QCM-D sequential experiments; see in Figure 3 the raw traces, where the HSA adsorbed onto the various unspecific and specific surfaces was allowed to interact with a 9.0 μg/mL anti-HSA solution. The experimentally measured ratios between the frequency shifts due to the anti-HSA uptake divided by the shifts due to the preadsorbed protein are reported in Figure 6.

The results show the highest anti-HSA/HSA ratio ($\geq$1) for the nonspecifically protein adsorbed onto UVO_3-Au and Tpy−SAM. By contrast, in the case of adsorption on Fe(II)-complex the ratio is ≅0.5 and for HSA onto Cu(II)-complexes the anti-

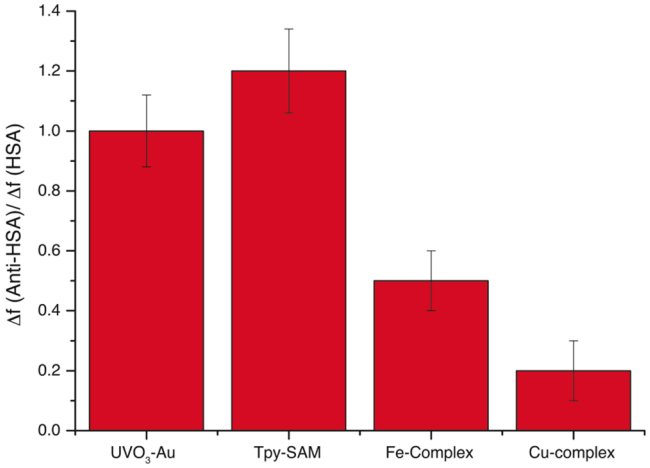

Figure 6. Ratios between the frequency shifts due to the anti-HSA uptake divided by the shifts due to the preadsorbed protein onto UVO_3-Au, Tpy−SAM, Fe-complex, Cu-complex.

DOI: 10.1021/acsami.5b08217
ACS Appl. Mater. Interfaces 2015, 7, 23353−23363

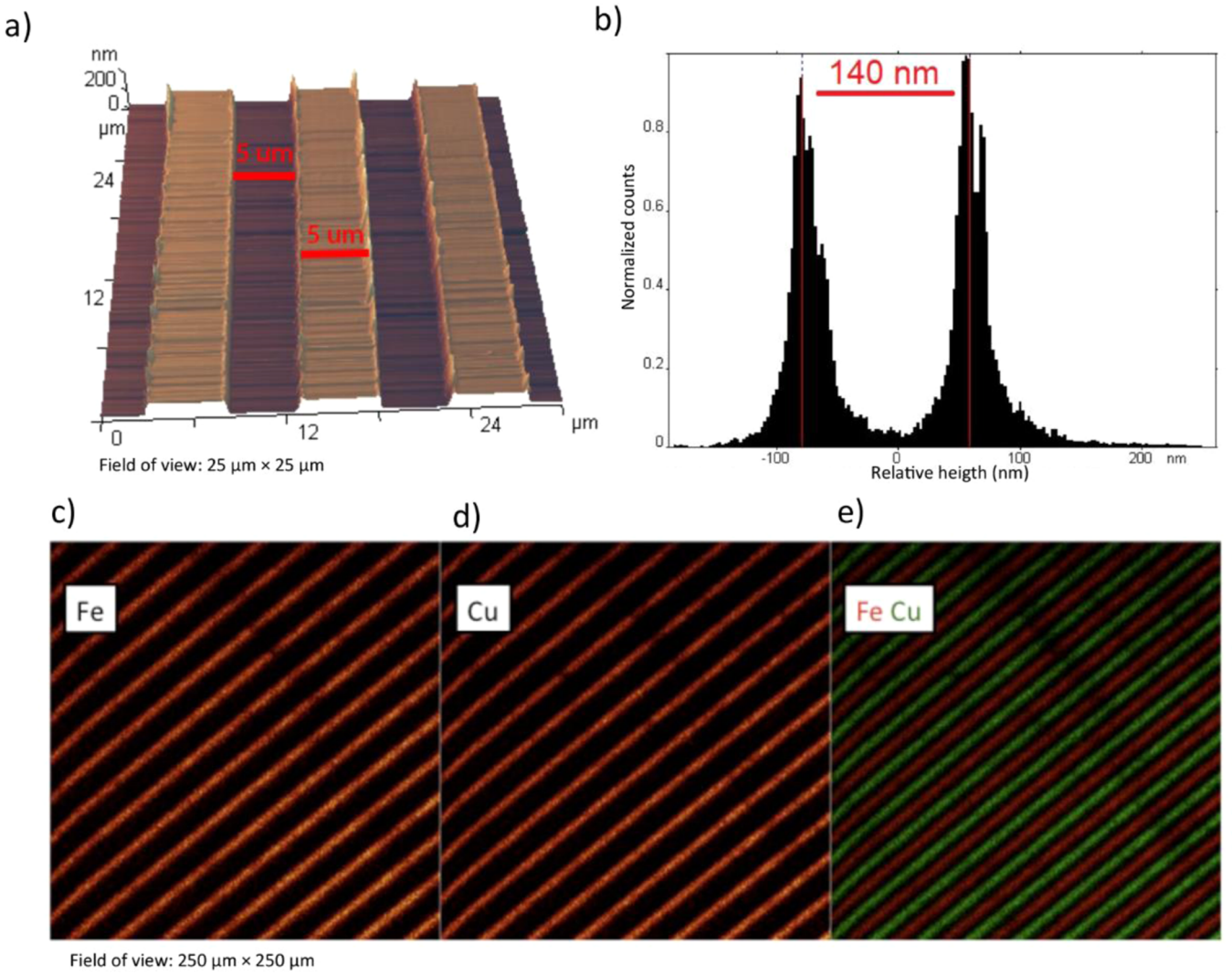

Figure 7. Topographic and chemical mapping. Portion a reports AFM topographic images indicating the width and distance between the gold stripes. Portion b shows the histogram analysis indicating the height of the stripes (140 nm). Remaining portions report false colors mass-resolved chemical maps of gold stripes selectively covered by Fe(II)- and Cu(II)-complexes. (c) Reports map of $^{56}Fe^{+}$. (d) Reports map of $^{63}Cu^{+}$. (e) Reports the two-color overlay of $^{56}Fe^{+}$ (red) and $^{63}Cu^{+}$ (green). Field of view: 250 μm × 250 μm.

HSA/HSA ratio is the lowest, i.e., ≅0.2. According to the specific ability of the anti-HSA of recognizing the denatured HSA molecules, the results confirm the above proposed hypothesis that HSA adsorbed onto nonspecific surfaces, including Fe(II)-complex, is mostly or completely denatured, while the HSA adsorbed onto the chelating Cu(II)-complexes is mostly in the native state.

These results lead to a global picture highlighting the crucial and selective role of the chelation process. Indeed, for the Cu(II) chelating ions, a very effective interaction occurs, based on very high Cu(II)-HSA binding affinity,[25] while for the Fe(II) ions the binding process is less effective, due to possible lower binding affinity, yielding a much lower HSA binding and a correspondingly higher denaturation of the adsorbed molecules.

3.3. Patterning Protein Biofunctionality. The preferential adsorption of HSA onto chelating surfaces in different conformational states has been exploited to patterning different biological functionality of the protein, retaining its own native state in case of the Cu(II)-complex surfaces and the mostly denatured state for the analogous Fe(II)-complex based ones.

Microstructured protein films were prepared by means of a novel mode of metal-complexes patterning, based on the versatile experimental platform outlined in Scheme 1.

The terpyridine-based self-assembled monolayers (SAMs) are formed onto arrays of interdigitated gold electrodes (see atomic force microscopy images in Figure 7a,b). These can be biased positively or negatively in alternating sequence. By dipping of the interdigitated electrodes in a Cu(II) containing solution, the Cu(II)-complex SAM is formed selectively at the negative biased electrodes, because of the electrostatic attraction toward the positive metal ions, while the terpyridine-moieties at the positively charges electrodes remain copper-free. Subsequently, the same sample is immersed in a Fe(II) containing solution without any bias. Since Cu(II) exhibits very strong interaction with terpyridine-based ligands, it forms very stable coordination complexes that resist the successive exchange reaction with Fe(II). Consequently, Fe(II)-complexes are formed selectively at the free-terpyridine SAM stripes. In such a way, we prepared a patterned surface that is decorated with Cu(II)-complex stripes lying beside Fe(II)-complex decorated ones.

DOI: 10.1021/acsami.5b08217
ACS Appl. Mater. Interfaces 2015, 7, 23353−23363

ToF-SIMS chemical imaging (Figure 7c–e) demonstrated the successful preparation of stripes of gold alternating and selectively covered by Fe(II) and Cu(II) complexes according to the protocol depicted in Scheme 1. Indeed the chemical maps of Figure 7b and Figure 7c, as well as their overlay (Figure 7d), show that coppers does not adsorb significantly on the positively biased gold stripes and that the subsequent treatment with iron, while "filling" the free terpyridine functions, does not interfere appreciably with the stripes already saturated with copper.

After dipping the bicomponent Cu(II)-/Fe(II)-complex-based micropatterns in protein solution and after a vigorous washing step, ToF-SIMS chemical maps were acquired. Figure 8 reports the elemental maps of Fe and Cu (Figure 8a and

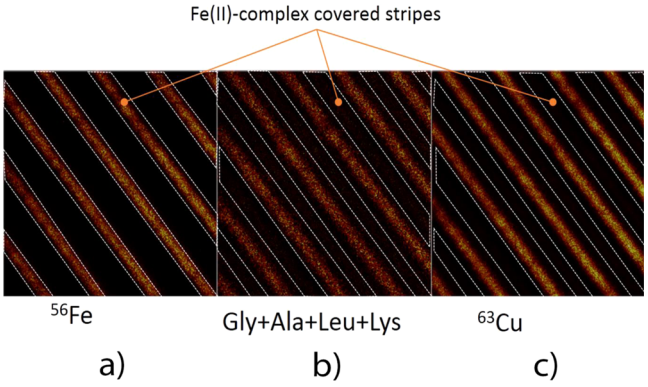

Figure 8. False color mass-resolved chemical maps of a typical patterned sample after incubation in HSA solution: (a) reports map of $^{56}Fe^{+}$; (b) reports map related to the sum of typical fragments of Gly, Ala, Leu, and Lys; (c) reports map of $^{63}Cu^{+}$. Field of view: 100 μm × 100 μm.

Figure 8c) together with the chemical map (Figure 8b) that represent the distribution of the sum of intensities of the characteristic amino acid fragments of HSA (glycine, alanine, leucine, and lysine fragments). The comparison of such images to each other clearly indicates that Fe(II)- and Cu(II)-based complexes essentially lie onto alternating gold stripes and that the distribution of the protein fragments is superimposed only to that of ^{56}Cu ion.

Furthermore, due to the almost complete loss of the HSA signals from the Fe(II)-based stripes, we can argue that the HSA molecules are easily removed from these stripes, while, owing the strong chelation binding of HSA with Cu(II)-complex, the protein remains selectively anchored at the chelating stripes (in spite of strong water rinsing), finally yielding very stable micropatterned native state HSA films.

4. CONCLUSIONS

In the present paper we have shown that the new "soft" strategy, based on highly selective ion metal chelation processes, may be employed to preserve the adsorbing proteins from the ubiquitous surface-induced major unfolding. By selecting the appropriate metal ions and suitable chelating molecules, it is possible to "attach" a protein in its native state to any functionalized substrate.

This is due to the fact that in the present work the chelating Cu(II)–protein interaction apparently allows a sort of "soft" protein landing, which not only is able to prevent the typical denaturation during the surface adsorption but also provides orientation information to the protein, owing to the highly specific symmetry facts, i.e., square planar complexing symmetry, of the metal ion–protein complex (see above). Furthermore, this "soft" landing apparently promotes a very efficient packing of the anchored HSA molecules resulting in a factor 2 in the amount of immobilized protein. The kinetic data further support the strong difference among HSA adsorption onto Cu(II)-chelated surfaces and onto Fe(II)-chelated surfaces, terpyridine and Au bare substrates, respectively. The HSA adsorption occurs indeed in two subsequent steps, without significant reorganization or denaturation.

The effective capacity of immobilizing denatured (onto Fe(II)-complexes) vs native state HSA (onto the chelating Cu(II)-complexes) has been unequivocally confirmed by in situ selective molecular recognition of denatured HSA with a monoclonal HSA-antibody.

The much higher stability of HSA anchored onto Cu(II)-chelating surfaces with respect to the protein anchored onto Fe(II)-complexed or the other unspecific surfaces (bare Au, terpyridine SAM) was finally exploited to obtain patterns of native state protein. It is noteworthy that the HSA patterns onto Cu(II)-chelated surfaces appear very robust, resisting energetic rinsing, while a simple washing step was sufficient to almost completely remove HSA linked to Fe(II).

Further work is being undertaken in two synergic directions, involving respectively the translation of the metal ion chelation methodology to metal oxides and polymeric surfaces and the extension of the described anchoring and patterning strategy of native state proteins to other relevant classes of cell-adhesive proteins, like fibronectin and vitronectin, to promote specific processes of cell ordering on the biomaterial or biodegradable scaffold surfaces.

AUTHOR INFORMATION

Corresponding Author

*E-mail: n.tuccitto@unict.it.

Funding

Authors gratefully acknowledge the financial support of the MIUR Projects PRIN 2010-11 No. 2010L9SH3K_002 and No. 2010N3T9M4_004 for funding and Optel InP grant at CSGI.

Notes

The authors declare no competing financial interest.

REFERENCES

(1) Gray, J. J. The Interaction Of Proteins With Solid Surfaces. *Curr. Opin. Struct. Biol.* **2004**, *14*, 110–115.

(2) Place, E. S.; Evans, N. D.; Stevens, M. M. Complexity In Biomaterials For Tissue Engineering. *Nat. Mater.* **2009**, *8*, 457–470.

(3) Aminian, A.; Pardun, K.; Volkmann, E.; Li Destri, G.; Marletta, G.; Treccani, L.; Rezwan, K. Enzyme-Assisted Calcium Phosphate Biomineralization On An Inert Alumina Surface. *Acta Biomater.* **2015**, *13*, 335–343.

(4) Wang, K.; Zhou, C.; Hong, Y.; Zhang, X. A Review Of Protein Adsorption On Bioceramics. *Interface Focus* **2012**, *2*, 259–277.

(5) Marletta, G.; Ciapetti, G.; Satriano, C.; Perut, F.; Salerno, M.; Baldini, N. Improved Osteogenic Differentiation Of Human Marrow Stromal Cells Cultured On Ion-Induced Chemically Structured Poly-E-Caprolactone. *Biomaterials* **2007**, *28*, 1132–1140.

(6) Bryers, J. D.; Giachelli, C. M.; Ratner, B. D. Engineering Biomaterials To Integrate And Heal: The Biocompatibility Paradigm Shifts. *Biotechnol. Bioeng.* **2012**, *109*, 1898–1911.

(7) Dvir, T.; Timko, B. P.; Kohane, D. S.; Langer, R. Nanotechnological Strategies For Engineering Complex Tissues. *Nat. Nanotechnol.* **2011**, *6*, 13–22.

DOI: 10.1021/acsami.5b08217
ACS Appl. Mater. Interfaces 2015, 7, 23353–23363

(8) Gomes, S.; Leonor, I. B.; Mano, J. F.; Reis, R. L.; Kaplan, D. L. Natural And Genetically Engineered Proteins For Tissue Engineering. *Prog. Polym. Sci.* **2012**, *37*, 1−17.
(9) Yi, S. J.; Yuk, J. S.; Jung, S. H.; Zhavnerko, G. K.; Kim, Y. M.; Ha, K. S. Investigation of Selective Protein Immobilization On Charged Protein Array By Wavelength Interrogation-Based SPR Sensor. *Mol. Cells* **2003**, *15*, 333−340.
(10) Elsadek, B.; Kratz, F. Impact Of Albumin On Drug Delivery-New Applications On The Horizon. *J. Controlled Release* **2012**, *157*, 4−28.
(11) Tagaya, M.; Ikoma, T.; Hanagata, N.; Tanaka, J. Analytical Investigation Of Protein Mediation Between Biomaterials And Cells. *Mater. Express* **2012**, *2*, 1−22.
(12) Kunzmann, A.; Andersson, B.; Thurnherr, T.; Krug, H.; Scheynius, A.; Fadeel, B. Toxicology Of Engineered Nanomaterials: Focus On Biocompatibility, Biodistribution And Biodegradation. *Biochim. Biophys. Acta, Gen. Subj.* **2011**, *1810*, 361−373.
(13) Nakanishi, K.; Sakiyama, T.; Imamura, K. On The Adsorption Of Proteins On Solid Surfaces, A Common But Very Complicated Phenomenon. *J. Biosci. Bioeng.* **2001**, *91*, 233−244.
(14) Giamblanco, N.; Zhavnerko, G.; Tuccitto, N.; Licciardello, A.; Marletta, G. Coadsorption-Dependent Orientation Of Fibronectin Epitopes At Hydrophilic Gold Surfaces. *Soft Matter* **2012**, *8*, 8370−8378.
(15) Keselowsky, B. G.; Collard, D. M.; García, A. J. Surface Chemistry Modulates Fibronectin Conformation and Directs Integrin Binding and Specificity To Control Cell Adhesion. *J. Biomed. Mater. Res.* **2003**, *66*, 247−259.
(16) Anand, G.; Sharma, S.; Dutta, A. K.; Kumar, S. K.; Belfort, G. Conformational Transitions Of Adsorbed Proteins On Surfaces Of Varying Polarity. *Langmuir* **2010**, *26*, 10803−10811.
(17) Michael, K. E.; Vernekar, V. N.; Keselowsky, B. G.; Meredith, J. C.; Latour, R. A.; Garcia, A. J. Adsorption-Induced Conformational Changes In Fibronectin Due To Interactions With Well-Defined Surface Chemistries. *Langmuir* **2003**, *19*, 8033−8040.
(18) Vieira, E. P.; Rocha, S.; Pereira, M. C.; Moehwald, H.; Coelho, M. A. N. Adsorption And Diffusion Of Plasma Proteins On Hydrophilic And Hydrophobic Surfaces: Effect Of Trifluoroethanol On Protein Structure. *Langmuir* **2009**, *25*, 9879−9886.
(19) Giamblanco, N.; Martines, E.; Marletta, G. Laminin Adsorption On Nanostructures: Switching The Molecular Orientation By Local Curvature Changes. *Langmuir* **2013**, *29*, 8335−8342.
(20) Keller, T. F.; Schönfelder, J.; Reichert, J.; Tuccitto, N.; Licciardello, A.; Messina, G. M. L.; Marletta, G.; Jandt, K. D. How The Surface Nanostructure Of Polyethylene Affects Protein Assembly And Orientation. *ACS Nano* **2011**, *5*, 3120−3131.
(21) Tuccitto, N.; Giamblanco, N.; Licciardello, A.; Marletta, G. Patterning Of Lactoferrin Using Functional Sams Of Iron Complexes. *Chem. Commun.* **2007**, *25*, 2621−2623.
(22) Giamblanco, N.; Tuccitto, N.; Licciardello, A.; Marletta, G. Focused Ion Beam Treatment Of Self-Assembled Monolayers For Protein Patterning. *Eur. Cells Mater.* **2007**, *14*, 32.
(23) Tuccitto, N.; Giamblanco, N.; Ghosh, S.; Spampinato, V.; Labbé, P.; Dumy, P.; Quici, S.; Marletta, G.; Defrancq, E.; Licciardello, A. Controlled Density Patterning Of Tolylterpyridine-Tagged Oligonucleotides. *Langmuir* **2011**, *27*, 8595−8599.
(24) Ali, M.; Nasir, S.; Nguyen, Q. H.; Sahoo, J. K.; Tahir, M. N.; Tremel, W.; Ensinger, W. Metal Ion Affinity-Based Biomolecular Recognition And Conjugation Inside Synthetic Polymer Nanopores Modified With Iron-Terpyridine Complexes. *J. Am. Chem. Soc.* **2011**, *133*, 17307−17314.
(25) Fanali, G.; di Masi, A.; Trezza, V.; Marino, M.; Fasano, M.; Ascenzi, P. Human Serum Albumin: From Bench To Bedside. *Mol. Aspects Med.* **2012**, *33*, 209−290.
(26) Zvimba, J. N. Copper Chelating Anti-Inflammatory Agents of Pseudo-Mimics of Human Serum Albumin (HSA): Copper and Rheumatoid Arthritis. Ph.D. Thesis, University of Cape Town, South Africa, 2005.
(27) Carter, D. C.; Ho, J. X. Structure Of Serum Albumin. *Adv. Protein Chem.* **1994**, *45*, 153−203.
(28) Sadler, P. J.; Tucker, A.; Viles, J. H. Involvwment Of A Lysibe Residue In The N-Terminal Ni2+ And Cu2+ Binding-Site Of Serum Albumins Comparison With Co2+, Cd2+ And Al3+. *Eur. J. Biochem.* **1994**, *220*, 193−200.
(29) De Silva, S.; De Silva, R. M.; De Silva, K. M. N. Molecular Mechanics (MM), Molecular Dynamics (MD) And Semi-Empirical Study Of Co^{2+}, Cu^{2+}, Ni^{2+} And Cd^{2+} Binding To N-Terminal Of Human Serum Albumin (HSA). *J. Mol. Struct.: THEOCHEM* **2004**, *711*, 73−81.
(30) Laussac, J. P.; Sarker, B. Characterization Of The Copper(II)- And Nickel(II)-Transport Site Of Human Serum Albumin. Studies Of Copper(II) And Nickel(II) Binding To Peptide 1−24 Of Human Serum Albumin By 13C And 1H NMR Spectroscopy. *Biochemistry* **1984**, *23*, 2832−2838.
(31) Wang, R.; Wang, W.; Ren, H.; Chae, J. Detection Of Copper Ions In Drinking Water Using The Competitive Adsorption Of Proteins. *Biosens. Bioelectron.* **2014**, *57*, 179−185.
(32) Maalouli, N.; Gouget-Laemmel, A. C.; Pinchemel, B.; Bouazaoui, M.; Chazalviel, J.; Ozanam, F.; Yang, Y.; Burkhard, P.; Boukherroub, R.; Szunerits, S. Development Of A Metal-Chelated Plasmonic Interface For The Linking Of His-Peptides With A Droplet-Based Surface Plasmon Resonance Read-Off Scheme. *Langmuir* **2011**, *27*, 5498−5505.
(33) Kanazawa, K. K.; Gordon, J. G. Frequency Of A Quartz Microbalance In Contact With Liquid. *Anal. Chem.* **1985**, *57*, 1770−1771.
(34) Sauerbrey, G. Verwendung Von Schwingquarzen Zur Wägung Dünner Schichten Und Zur Mikrowägung. *Eur. Phys. J. A* **1959**, *155*, 206−222.
(35) Sigal, G. B.; Bamdad, C.; Barberis, A.; Strominger, J.; Whitesides, G. M. A Self-Assembled Monolayer For The Binding And Study Of Histidine Tagged Proteins By Surface Plasmon Resonance. *Anal. Chem.* **1996**, *68*, 490−497.
(36) Prime, K. L.; Whitesides, G. M. Adsorption Of Proteins Onto Surfaces Containing End-Attached Oligo(Ethylene Oxide) - A Model System Using Self-Assembled Monolayers. *J. Am. Chem. Soc.* **1993**, *115*, 10714−10721.
(37) Auditore, A.; Tuccitto, N.; Marzanni, G.; Quici, S.; Puntoriero, F.; Campagna, S.; Licciardello, A. Organized Assemblies Of Thiol-Terpyridine And Thiophenol On Gold Surfaces: Preferential Composition Of Mixed Species Evidenced. *Chem. Commun.* **2003**, *9*, 2494−2495.
(38) Auditore, A.; Tuccitto, N.; Quici, S.; Marzanni, G.; Puntoriero, F.; Campagna, S.; Licciardello, A. ToF-SIMS Investigation Of Functional Mixed Aromatic Thiol Monolayers On Gold. *Appl. Surf. Sci.* **2004**, *231−232*, 314−317.
(39) Battocchio, C.; Polzonetti, G.; Gambino, L.; Tuccitto, N.; Licciardello, A.; Marletta, G. Comparison Between Angular Dependent NEXAFS Analysis And Theoretical Calculations Of Molecular Orientation Of New Functional Mixed Aromatic Molecules Deposited Onto Au/Si(1 1 1). *Nucl. Instrum. Methods Phys. Res., Sect. B* **2006**, *246*, 145−150.
(40) Tuccitto, N.; Torrisi, V.; Cavazzini, M.; Morotti, T.; Puntoriero, F.; Quici, S.; Campagna, S.; Licciardello, A. Stepwise Formation Of Ruthenium(II) Complexes By Direct Reaction On Organized Assemblies Of Thiol-Terpyridine Species On Gold. *ChemPhysChem* **2007**, *8*, 227−230.
(41) Tuccitto, N.; Torrisi, V.; Delfanti, I.; Licciardello, A. Monoatomic And Cluster Beam Effect On Tof-SIMS Spectra Of Self-Assembled Monolayers On Gold. *Appl. Surf. Sci.* **2008**, *255*, 874−876.
(42) Tuccitto, N.; Delfanti, I.; Torrisi, V.; Scandola, F.; Chiorboli, C.; Stepanenko, V.; Würthner, F.; Licciardello, A. Supramolecular Self-Assembled Multilayers Of Terpyridine-Functionalized Perylene Bisimide Metal Complexes. *Phys. Chem. Chem. Phys.* **2009**, *11*, 4033−4038.

DOI: 10.1021/acsami.5b08217
ACS Appl. Mater. Interfaces 2015, 7, 23353−23363

(43) Tuccitto, N.; Ferri, V.; Cavazzini, M.; Quici, S.; Zhavnerko, G.; Licciardello, A.; Rampi, M. A. Highly Conductive ~ 40-Nm-Long Molecular Wires Assembled By Stepwise Incorporation Of Metal Centres. *Nat. Mater.* **2009**, *8*, 41−46.
(44) Spampinato, V.; Tuccitto, N.; Quici, S.; Calabrese, V.; Marletta, G.; Torrisi, A.; Licciardello, A. Functionalization Of Oxide Surfaces By Terpyridine Phosphonate Ligands: Surface Reactions And Anchoring Geometry. *Langmuir* **2010**, *26*, 8400−8406.
(45) Camillone, N.; Chidsey, C. E. D.; Liu, G. Y.; Scoles, G. Superlattice Structure At The Surface Of A Monolayer Of Octadecanethiol Self-Assembled On Au(111). *J. Chem. Phys.* **1993**, *98*, 3503−3511.
(46) Kozlowski, H.; Potocki, S.; Remelli, M.; Rowinska-Zyrek, M.; Valensin, D. Specific Metal Ion Binding Sites In Unstructured Regions Of Proteins. *Coord. Chem. Rev.* **2013**, *257*, 2625−2638.
(47) Sokolowska, M.; Krezel, A.; Dyba, M.; Szewczuk, Z.; Bal, W. Short Peptides Are Not Reliable Models Of Thermodynamic And Kinetic Properties Of The N-Terminal Metal Binding Site In Serum Albumin. *Eur. J. Biochem.* **2002**, *269*, 1323−1331.
(48) Kozlowski, H.; Bal, W.; Dyba, M.; Kowalik-Jankowska, T. Specific Structure-Stability Relations In Metallopeptides. *Coord. Chem. Rev.* **1999**, *184*, 319−346.
(49) Azizian, S. Kinetic Models Of Sorption: A Theoretical Analysis. *J. Colloid Interface Sci.* **2004**, *276*, 47−52.
(50) Glaser, R. W. Antigen-Antibody Binding And Mass-Transport By Convection And Diffusion To A Surface - A 2-Dimensional Computer-Model Of Binding And Dissociation Kinetics. *Anal. Biochem.* **1993**, *213*, 152−161.
(51) Schuck, P. Kinetics Of Ligand Binding To Receptor Immobilized In A Polymer Matrix, As Detected With An Evanescent Wave Biosensor 0.1. A Computer Simulation Of The Influence Of Mass Transport. *Biophys. J.* **1996**, *70*, 1230−1249.
(52) Guo, M.; Zou, H. F.; Wang, H. L.; Kong, L.; Ni, J. Y. Binding Of Metal Ions With Protein Studied By A Combined Technique Of Microdialysis With Liquid Chromatography. *Anal. Chim. Acta* **2001**, *443*, 91−99.
(53) Bal, W.; Christodoulou, J.; Sadler, P. J.; Tucker, A. Multi-Metal Binding Site Of Serum Albumin. *J. Inorg. Biochem.* **1998**, *70*, 33−39.
(54) Paul, S.; Paul, D.; Basova, T.; Ray, A. K. Studies Of Adsorption And Viscoelastic Properties Of Proteins Onto Liquid Crystal Phthalocyanine Surface Using Quartz Crystal Microbalance With Dissipation Technique. *J. Phys. Chem. C* **2008**, *112*, 11822−11830.
(55) Fredriksson, C.; Kihlman, S.; Rodahl, M.; Kasemo, B. The Piezoelectric Quartz Crystal Mass And Dissipation Sensor: A Means Of Studying Cell Adhesion. *Langmuir* **1998**, *14*, 248−251.
(56) Rodahl, M.; Hook, F.; Fredriksson, C.; Keller, C. A.; Krozer, A.; Brzezinski, P.; Voinova, M.; Kasemo, B. Simultaneous Frequency And Dissipation Factor QCM Measurements Of Biomolecular Adsorption And Cell Adhesion. *Faraday Discuss.* **1997**, *107*, 229−46.
(57) Andersson, J.; Ekdahl, K. N.; Lambris, J. D.; Nilsson, B. Binding Of C3 Fragments On Top Of Adsorbed Plasma Proteins During Complement Activation On A Model Biomaterial Surface. *Biomaterials* **2005**, *26*, 1477−1485.
(58) Fischer, H.; Polikarpov, I.; Craievich, A. F. Average Protein Density Is A Molecular-Weight-Dependent Function. *Protein Sci.* **2004**, *13*, 2825−2828.
(59) Wang, X.; Herting, G.; Wallinder, I. O.; Blomberg, E. Adsorption Of Bovine Serum Albumin On Silver Surfaces Enhances The Release Of Silver At pH Neutral Conditions. *Phys. Chem. Chem. Phys.* **2015**, *17*, 18524−18534.
(60) Pignataro, B.; Marletta, G. Nanoscale Organization Of Human Serum Albumin At Model Cytocompatible Surfaces. *Mater. Sci. Eng., C* **2001**, *15*, 245−248.
(61) Product Information. Monoclonal Anti-Albumin, Clone HSA-11. Sigma-Aldrich: St. Louis, MO, 2015.

DOI: 10.1021/acsami.5b08217
ACS Appl. Mater. Interfaces 2015, 7, 23353−23363